Journal of Renewable Energy and Smart Systems *Vol.1, No.1, 2024: 47-54*

Renewable Energy and Smart Systems

journal homepage: https://sanad.iau.ir/journal/res

Controlled/Uncontrolled Rectifier Harmonic Modeling Using Differential Function Averaging Method

Atila Skandarnezhad[1,*], Noruz Abdollahi[1] , AbdolAziz Kalteh[1]

[1]*Department of Electrical Engineering, Aliabad Katoul Branch, Islamic Azad University, Aliabad Katoul, Iran*

Article info

Keywords:
Numerical Model
Recursive functions
Harmonic Components
Line Commutation
Differential Equation

Article history:
Received: 23 Apr 2024
Accepted: 10 Jul 2024

Abstract

Modeling techniques helps the designer to truly comprehend the internal variables of the system and construct the ultimate hardware precisely. This paper present a mathematical method based on the recursive differential equations in order to calculate the voltage and current harmonics of line commutated switching converters. Switches characteristic curves are nonlinear then traditional methods using linear approaches cannot be used for modeling purposes. Here, first the characteristic curve of the switches are rotated and then the related voltage-current diagram of the switches will be extracted. Then, the impedance and transmission matrices of the linear components will be determined using the traditional mesh and node methods. In the next step, the system block diagram of the converter which includes differential operators is determined. Here, using the recursive differential computation method based on the multivariable Runge-Kutta equation, the instantaneous values of the parameters will be calculated. Then, using the result of calculations, the off-state angles of the switches can be specified and amplitude of the harmonics up to the desired components can be determined and lastly, the ultimate numerical model will be extracted. Finally, the results of the simulation using the proposed method will be compared with the analytical-algebraic method. The results of comparison point out the performance of the suggested method for voltage and current estimation of the switches.

* Corresponding author.
*E-mail address :*eskandarnejad@aliabadiau.ac.ir

1. Introduction

Within industry, the ultimate cost of a switch is a determinative parameter. Due to this, in high-power rectifiers, usage of switches such as Thyristor and Triac are economically advantageous compared to other switches. The high-power rectifiers re used within application like welding machine, HVDC, remote control, etc. [1]. The aim of the modeling is to determine an equivalent circuit for the switch so that it can substitute the switch while showing the actual state of the characteristics of the electrical circuit. Here, the better the modeling would be, the more precise estimation capability of the operation point of the switch is [2]. For switches in which the conduction interval or their on-off timing are specified, the modeling process is easier, however, for thyristor and triac it can be more complicated since although their firing angles are given, but the extinction angle is dependent on the circuit conditions [3]. The traditional method to determine the voltage and current of the switches in converters is to state the corresponding differential equations and solve them. Nonetheless, as the number of the switches increases, finding the solution become cumbersome. The solution includes two components which are the permanent and transient parts even though in the rectifier power analysis, only the permanent characteristic is important. On the other hand, for higher powers, it can be claimed with acceptable approximation that most of the signal power is included within the first three components of the Fourier series, that is, the DC part of the signal and the first and second harmonics [4].

There are various method to describe linearly the nonlinear devices, however, these method are mostly complicated and of low performance. In the ideal case, the semiconductor switches can be seen as a switch that is in on and off state, each for a while [5]. When the on and off periods of the switch and the equivalent impedance across it are known, the voltage and current harmonics of the switch can be determined for each frequency and harmonic independently. Here, using the vector-matrix operations, values of the active and reactive powers of each component can be obtained. We assume that other than the switches within the circuit, the rest of the devices are all linear. If a model is presented for a triac, it can be used for the thyristor family too [6].

2. Rotated Switch Characteristic Curve

The characteristic curve of triac is shown in fig. 1.

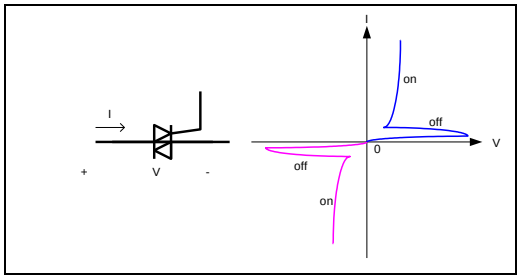

Fig. 1: The characteristic Curve of Triac

Also, its states of voltage and current for an ideal on and off case are depicted in fig. 2 [7].

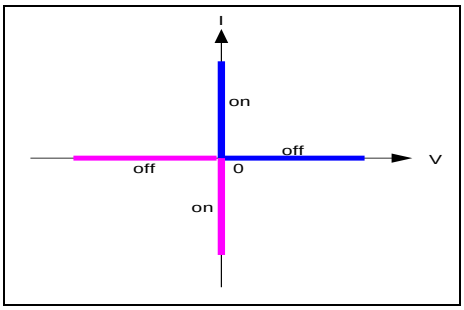

Fig. 2: The Ideal Characteristic Curve

This curve can be interpreted as two perpendicular line, one for V = 0 for on state and the other for I = 0 in off state. When the curve in fig. 2 is rotated 45 degrees clockwise, the curve in fig. 3 would be obtained [8]. This curve is combined of two line segment, one from the relation I'=V' for the on state and I'=-V' for the off state. The length of each line segment within the curve is proportional to the applied voltage, firing angle and amplitude of the flowing current. The operating point of the switch at each moment is located on one of the line segments and when it changes into another operating point, it must cross in the coordinated system [8].

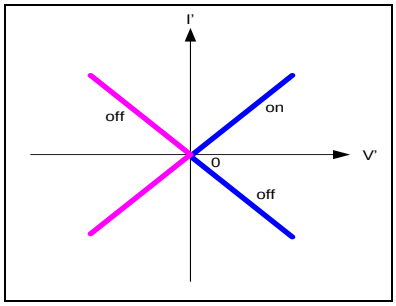

Fig. 3: The Ideal Rotated characteristic Curve

The Rotation matrix and its inverse are respectively denoted by T and T'. The analysis of the switch behavior using two different individual matrices makes the modeling process easier. Now, the traic behavior can be described using the matrix transformation in fig. 4. Using the rotation, the I-V curve would be transformed into a function which facilitate the finding the equations' solutions.

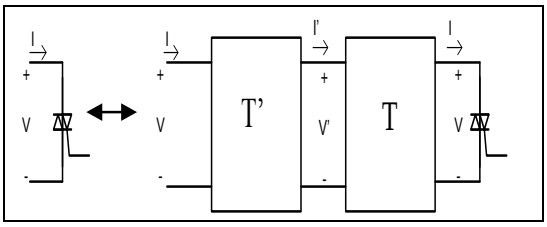

Fig. 4: The Equivalent Block of the Triac

The T and T' matrices along with the related transformations are stated in (1) and (2), which can be inserted into the block diagram, correspondingly.

$$\begin{bmatrix} V' \\ I' \end{bmatrix} = [T] \begin{bmatrix} V \\ I \end{bmatrix} \quad , T = \frac{1}{\sqrt{2}} \begin{bmatrix} 1 & 1 \\ -1 & 1 \end{bmatrix} \tag{1}$$

$$\begin{bmatrix} V \\ I \end{bmatrix} = [T'] \begin{bmatrix} V' \\ I' \end{bmatrix} \quad , T' = \frac{1}{\sqrt{2}} \begin{bmatrix} 1 & -1 \\ 1 & 1 \end{bmatrix} \tag{2}$$

Multiplication of T and T' gives the identity matrix I. Even through using the ideal curve in fig. 2 instead of the actual characteristic curve in fig. 1 causes some error in the subsequent equations, the value of this error is negligible. Because the line commutation here mostly is used in converter of high powers, the mentioned error would be very small and insignificant. Also, the voltage loss across the switch and its inverse saturated current are negligible compared to the converter current [9].

The characteristic curve presented here can be generalized to all the switches of thyristor family; the firing time in all members is arbitrary and extinction time is determined by the line commutation conditions [10]. The reason behind choosing traic, is that it is bidirectional and second its characteristic curve is more general; it goes without saying that the modeling process presented here has similar routine for all the members of the triac family [11].

In order to estimate the extinction angle of the switch, the resulted mathematical equations of the transformation matrices will be expanded.

3. Switch's Voltage and Current calculation

To determine voltage and current of the switch, the third and higher order harmonics will be neglected from consideration. This assumption is totally safe for high powers [12]. To find a unique solution, the calculations are done in the I'-V' coordination; thus, the Fourier expansion of the switch's voltage and current can be computed using (3) and (4).

$$V'(t) \cong V'_0 + V'_1 \sin(\omega t + \phi'_1) + V'_2 \sin(2\omega t + \phi'_2) \tag{3}$$

$$I'(t) \cong I'_0 + I'_1 \sin(\omega t + \psi'_1) + I'_2 \sin(2\omega t + \psi'_2) \tag{4}$$

The on/off interval of the switch shown in fig. 5.

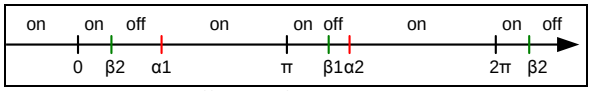

Fig. 5: on and off states of the switch within one period

In fig. 5, a_1 and a_2, respectively, denote the firing angles in the positive and negative half-period and b_1 and b_2 are their corresponding extinction angles. As the triac goes to the off state when the line commutation occurs, the voltage loss across the switch and its holding current are assumed to be zero. The triac goes to off state when the anode-cathode voltage becomes zero. Thus, given the firing angles, the extinction angles can be determined through solving the equation V'(t) = 0 [13]. Therefore, by expansion of (3), the relation (5) can be derived. Then, solving (5) and determining the true solutions gives the extinction angles [14].

$$\kappa_4 \sin^4(\omega t) + \kappa_3 \sin^3(\omega t) + \kappa_2 \sin^2(\omega t) + \kappa_1 \sin^1(\omega t) + \kappa_0 = 0 \Rightarrow$$

$$\kappa_4 = 4V'^2_2$$

$$\kappa_3 = 4V'_1 V'_2 \sin(\phi'_1 - \phi'_2) \tag{5}$$

$$\kappa_2 = V'^2_1 - 4V'^2_2 - 4V'_0 V'_2 \sin\phi'_2$$

$$\kappa_1 = 2V'_1 (V'_2 \sin(\phi'_2 - \phi'_1) + V'_0 \cos\phi'_1 - V'_2 \sin\phi'_1 \cos\phi'_2)$$

$$\kappa_0 = (V'^2_2 - V'^2_1) \sin^2\phi'_2 + V'^2_0 + 2V'_0 V'_2 \sin\phi'_2$$

Since when the switch is on we have I'=V' and when it is off, I'=-V', the 0'th and 1'th and 2'th harmonic component can be calculated where the sine and cosine parts can be expressed as in (6)-(12) through the following equations.

$$I'_0 = \frac{1}{2\pi}\int_0^{2\pi} I'(t)d(\omega t) \quad (6)$$

$$I'_{1C} = \frac{1}{\pi}\int_0^{2\pi} I'(t)\cos(\omega t)d(\omega t) \quad (7)$$

$$I'_{1S} = \frac{1}{\pi}\int_0^{2\pi} I'(t)\sin(\omega t)d(\omega t) \quad (8)$$

$$I'_1 = \sqrt{I'^{\,2}_{1C} + I'^{\,2}_{1S}}\ ;\ \psi'_1 = \tan^{-1}\left(\frac{I'_{1S}}{I'_{1C}}\right) \quad (9)$$

$$I'_{2C} = \frac{1}{\pi}\int_0^{2\pi} I'(t)\cos(2\omega t)d(\omega t) \quad (10)$$

$$I'_{2S} = \frac{1}{\pi}\int_0^{2\pi} I'(t)\sin(2\omega t)d(\omega t) \quad (11)$$

$$I'_2 = \sqrt{I'^{\,2}_{2C} + I'^{\,2}_{2S}}\ ;\ \psi'_2 = \tan^{-1}\left(\frac{I'_{2S}}{I'_{2C}}\right) \quad (12)$$

Where, I_0 is the DC component of the current, I_s, the sine component, I_c, the cosine component and ψ', the angle of the corresponding component. The parametric solution of the extinction angles are expressed in (13).

$$V'(t) = 0 \ \Rightarrow\ \beta_1, \beta_2\ ;\ \frac{dV'(\beta_1)}{dt} \prec 0, \frac{dV'(\beta_2)}{dt} \succ 0 \quad (13)$$

In the equation, in the first extinction angle β_1, the slope of the voltage is negative while in the second, β_2, the slope of the voltage is positive. Therefore, the current components are determined in terms of the voltage, which are expressed in (14)-(18) after some manipulation. In the following relations, α is the firing angle, β, the extinction angle and ψ the phase difference. Also, the indices 1 and 2 denote the first and second half-cycles. Eqs. (15)-(16) are for the first component and (17)-(18) for the second one.

$$I'_0 = \frac{V'_0}{\pi}(\pi + \beta_2 + \beta_1 - \alpha_2 - \alpha_1) +$$
$$\frac{V'_1}{\pi}(\cos(\alpha_1 + \phi'_1) + \cos(\alpha_2 + \phi'_1) - \cos(\beta_1 + \phi'_1) - \cos(\beta_2 + \phi'_1)) +$$
$$\frac{V'_2}{2\pi}(\cos(2\alpha_1 + \phi'_2) + \cos(2\alpha_2 + \phi'_2) - \cos(2\beta_1 + \phi'_2) - \cos(2\beta_2 + \phi'_2)) \quad (14)$$

$$I'_{1C} = \frac{2V'_0}{\pi}(\sin\beta_2 + \sin\beta_1 - \sin\alpha_2 - \sin\alpha_1) +$$
$$\frac{V'_1}{\pi}(\pi + \beta_2 + \beta_1 - \alpha_2 - \alpha_1)\sin\phi'_1 +$$
$$\frac{V'_1}{2\pi}(\cos(2\alpha_1 + \phi'_1) + \cos(2\alpha_2 + \phi'_1) - \cos(2\beta_1 + \phi'_1) - \cos(2\beta_2 + \phi'_1)) +$$
$$\frac{V'_2}{\pi}(\cos(\alpha_1 + \phi'_2) + \cos(\alpha_2 + \phi'_2) - \cos(\beta_1 + \phi'_2) - \cos(\beta_2 + \phi'_2)) +$$
$$\frac{V'_2}{3\pi}(\cos(3\alpha_1 + \phi'_2) + \cos(3\alpha_2 + \phi'_2) - \cos(3\beta_1 + \phi'_2) - \cos(3\beta_2 + \phi'_2)) \quad (15)$$

$$I'_{1S} = \frac{-2V'_0}{\pi}(\cos\beta_2 + \cos\beta_1 - \cos\alpha_2 - \cos\alpha_1) +$$
$$\frac{V'_1}{\pi}(\pi + \beta_2 + \beta_1 - \alpha_2 - \alpha_1)\cos\phi'_1 +$$
$$\frac{V'_1}{2\pi}(\sin(2\alpha_1 + \phi'_1) + \sin(2\alpha_2 + \phi'_1) - sin(2\beta_1 + \phi'_1) - \sin(2\beta_2 + \phi'_1)) -$$
$$\frac{V'_2}{\pi}(\sin(\alpha_1 + \phi'_2) + \sin(\alpha_2 + \phi'_2) - \sin(\beta_1 + \phi'_2) - \sin(\beta_2 + \phi'_2)) +$$
$$\frac{V'_2}{3\pi}(\sin(3\alpha_1 + \phi'_2) + \sin(3\alpha_2 + \phi'_2) - \sin(3\beta_1 + \phi'_2) - \sin(3\beta_2 + \phi'_2)) \quad (16)$$

$$I'_{2C} = \frac{V'_0}{\pi}(\sin 2\beta_2 + \sin 2\beta_1 - \sin 2\alpha_2 - \sin 2\alpha_1) +$$
$$\frac{V'_2}{\pi}(\pi + \beta_2 + \beta_1 - \alpha_2 - \alpha_1)\sin\phi'_2 +$$
$$\frac{V'_2}{4\pi}(\cos(4\alpha_1 + \phi'_2) + \cos(4\alpha_2 + \phi'_2) - \cos(4\beta_1 + \phi'_2) - \cos(4\beta_2 + \phi'_2)) -$$
$$\frac{V'_1}{\pi}(\cos(\alpha_1 + \phi'_1) + \cos(\alpha_2 + \phi'_1) - \cos(\beta_1 + \phi'_1) - \cos(\beta_2 + \phi'_1)) +$$
$$\frac{V'_1}{3\pi}(\cos(3\alpha_1 + \phi'_1) + \cos(3\alpha_2 + \phi'_1) - \cos(3\beta_1 + \phi'_1) - \cos(3\beta_2 + \phi'_1)) \quad (17)$$

$$I'_{2S} = \frac{-V'_0}{\pi}(\cos 2\beta_2 + \cos 2\beta_1 - \cos 2\alpha_2 - \cos 2\alpha_1) +$$
$$\frac{V'_2}{\pi}(\pi + \beta_2 + \beta_1 - \alpha_2 - \alpha_1)\cos\phi'_2 +$$
$$\frac{V'_2}{4\pi}(\sin(4\alpha_1 + \phi'_2) + \sin(4\alpha_2 + \phi'_2) - \sin(4\beta_1 + \phi'_2) - \sin(4\beta_2 + \phi'_2)) -$$
$$\frac{V'_1}{\pi}(\sin(\alpha_1 - \phi'_1) + \sin(\alpha_2 - \phi'_1) - \sin(\beta_1 - \phi'_1) - \sin(\beta_2 - \phi'_1)) +$$
$$\frac{V'_1}{3\pi}(\sin(3\alpha_1 + \phi'_1) + \sin(3\alpha_2 + \phi'_1) - \sin(3\beta_1 + \phi'_1) - \sin(3\beta_2 + \phi'_1)) \quad (18)$$

4. Extraction of Converter Overall Model

Here a converter composing number of nonlinear switches and linear elements will be analyzed using the proposed method. The desired converter according to fig. 6 includes passive elements and a number of triacs and voltage and current sources.

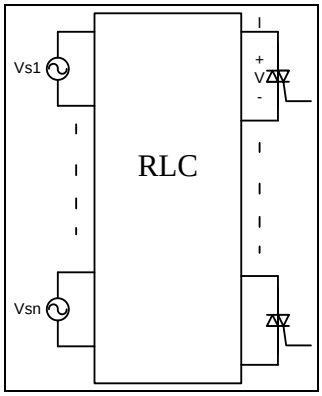

Fig. 6: The architecture of the converter with n switches

Using the matrix transformation in (1) and (2), the above circuit will be transformed to fig. 7.

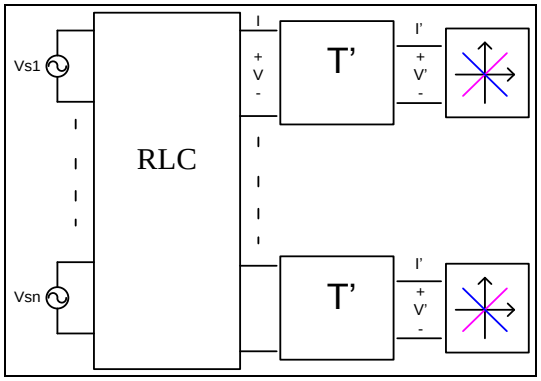

Fig. 7: The Equivalent transformed of the converter circuit in fig. 6

Now, given the admittance seen across the switch Y and inserting the values into the matrix T', the circuit in fig. 8 can be derived.

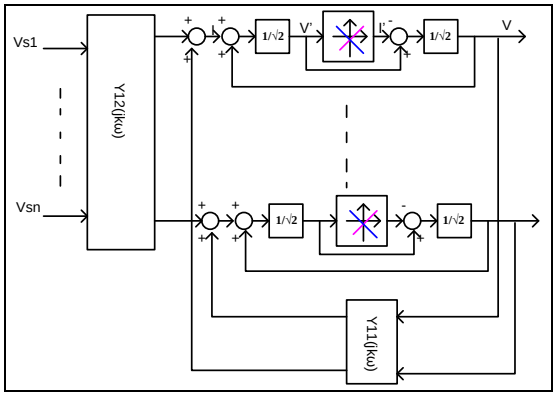

Fig. 8: The System Block Diagram of the Converter in fig. 6

The computations will be done only for the first three expressions of the current and voltage because computation for higher order expressions is time-consuming and complicated in one hand, and their values will not impact the solutions significantly, on the other. In (19), the transfer function of current to voltage is denoted by H'.

$$H'_0 = \frac{I'_0}{V'_0} \;;\; H'_1 = \frac{I'_1.e^{j\psi'_1}}{V'_1.e^{j\phi'_1}} \;;\; H'_2 = \frac{I'_2.e^{j\psi'_2}}{V'_2.e^{j\phi'_2}} \qquad (19)$$

With the insertion of (`9) into (8), the voltage and current harmonics for each switch are calculated and the system block diagram for the components is depicted as in fig. 9. In this block diagram, where the output I' is in terms of the variables V' and E, the parameter E is the harmonic component of the voltage source. By expanding the transformation matrix T as in (2) and adopting a process as in fig. 9, the block of fig. 10 can be derived in terms of I-V.

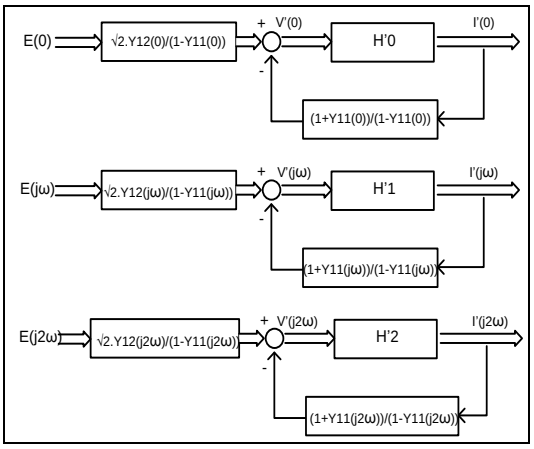

Fig. 9: The Block Diagram of each component in Terms of I'-V'

This block diagram encompasses recursive loop which is used for numerical calculation of harmonic components while it can be expanded for larger n.

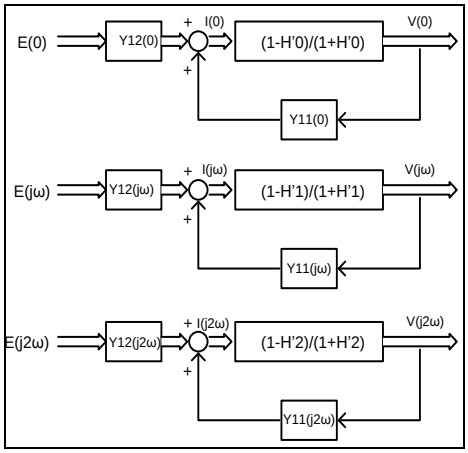

Fig. 10: The Block Diagram of each component in terms of I-V

The block diagrams shown in fig. 9 and fig. 10 are recursive function for numerical calculation of the harmonic components within the I'-V' or I-V spaces. Through enough iteration of the computational loop of the block diagrams 9 and 10, acceptable precision for each component in attainable. The recursive function in the I'-V' space is expressed in (20).

$$C_{11}(jn\omega)=\frac{1+Y_{11}(jn\omega)}{1-Y_{11}(jn\omega)}\ ;\ C_{12}(jn\omega)=\frac{\sqrt{2}\,Y_{12}(jn\omega)}{1-Y_{11}(jn\omega)} \quad (20)$$

The recursive function used for harmonic calculation and increasing the precision using function H is described in (21) as follows.

$$I'_n(\kappa)=H'_n(\kappa).V'_n(\kappa) \quad (21)$$

$$V'_n(\kappa+1)=-C_{11}(jn\omega).I'_n(\kappa)+C_{12}(jn\omega).E(jn\omega)$$

5. Proposing the Modeling Flowchart and a Typical Converter

In this section, the operating computational flowchart described before will be presented. Then, using a typical converter circuit, the results of the proposed method will be illustrated using computer simulation. The simulations of the proposed model and the corresponding circuit are, respectively, performed within the MATLAB and SPICE software packages. Fig. 11 shows the typical circuit here.

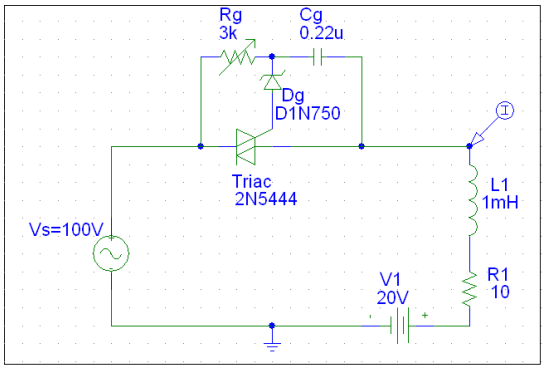

Fig. 11: The Typical Converter Circuit

The results of modeling methods and related simulations are given in table I, where it can be seen that the highest error is lower than 5%. The small difference of the results obtained through two methods given in table 1 is caused by the idealization of the I-V curve. Fig. 13 shows flowchart of the proposed method.

Table 1: Comparison of the Results of the Proposed Method

Simulation	Modeling	Converter Characteristics
α_1=072°	α_1=072°	Firing Angles
α_2=213°	α_2=213°	
β_1=170°	β_1=165°	Extinction Angles
β_2=372°	β_2=366°	
I_0=2.2A	I_0=2.1A	Current Components
I_1=8.6A	I_1=8.3A	
I_2=1.3A	I_2=1.2A	

Fig. 12 depicts the amplitude of the input harmonics.

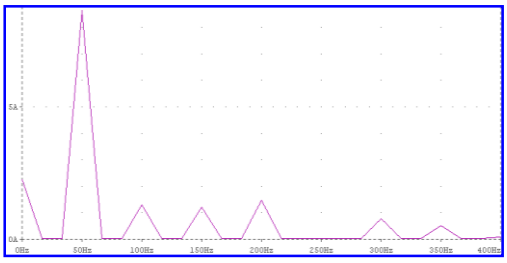

Fig. 12: The Amplitude of the Converter's Input Harmonics

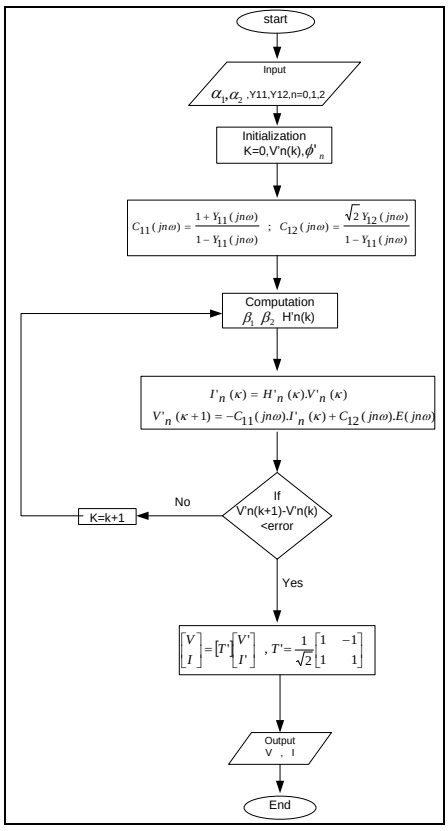

Fig. 13: Flowchart of the Proposed Modeling Method

Fig. 14 shows the voltage across the converter's load.

Fig. 14: Voltage across the Converter Output

Fig. 15 illustrates the current of the converter output which does not show any voltage spike due to the inductive load.

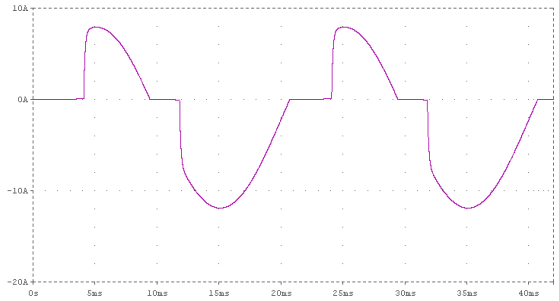

Fig. 15: Load Current of the converter output

6. Conclusion

In this paper, a numerical recursive method has been proposed to modeling the switches in line commutated converters. The proposed approach has high speed and precision; in addition, it can be combined with the computational algorithms included in circuit simulators so that convergence of the computational loop can be obtained within the minimum possible time. Results of the simulation along with their comparison with those of modeling are verifying these advantages. Values of the error in the results of the suggested method with respect to the actual ones are less than 5%. The method can be generalized for harmonic computation of higher orders too. It has been assumed that all the devices other than switches are linear. Since characteristic curve of such devices as diode, diac, thyristor, triac are similar to each other, thus the proposed method can be applied to a vast range of converter configurations. It should be noted that part of the ultimate error is resulted from the ideal assumption of the switch characteristic curve; this can be decreased using parasitic elements of the switch accordingly.

References

[A1] Nilsson SL, de Mattos Tenório AR, Sen S, Taylor A, Xu S, Zhao G, Song Q, Lei B ,"Application examples of the thyristor series capacitor". Flexible Transmission Systems: FACTS: 585–643, 2020.

[A2] G. T. Sayah, A. H. A. Zekry, H. F. Ragaie and F. A. Soliman, "A SPICE model of a thyristor with high injection effects and conductivity modulation," in Proc. 15th Int. Conf. on Microelectronics (ICM), pp. 344-347, Cairo, Egypt, Dec. 2003.

[A3] She X, Huang AQ, Lucía Ó, Ozpineci B, "Review of silicon carbide power devices and their applications". IEEE Trans Ind Electron 64:8193–8205, 2017.

[A4] J. Wang, Y. Du, S. Bhattacharya, and A. Q. Huang, "Characterization, modeling of 10-kV SiC JBS diodes and their application prospect in X-ray generators," IEEE Energy, 2012, 32(2): 234-242.

[A5] Vazquez S, Leon JI, Franquelo LG, Rodriguez J, Young HA, Marquez A, Zanchetta P ,"Model predictive control: a review of its applications in power electronics". IEEE Electron Mag 16–31, 2014.

[A6] Paisana, J. and Abreu Santos, H., "Applications of phase-plane analysis to thyristor modeling ", COMPEL-The international journal for computation and mathematics in electrical engineering, 26(4), pp. 1134-1141, 2007.

[A7] Z. Song, Y. Huo, and Y. Pang, "The research on transient analysis and auxiliary circuit of power thyristor," in proc. 4th. Int. Conf. on Electric Utility, DRPT, pp. 1667-1670, Shandong, China, 2011.

[A8] C. P. Basso, Switch Mode Power Supplies: SPICE Simulation and Practical Designs, 1nd Edition, McGraw - Hill, pp. 100-108, 2008.

[A9] S. B. Tiab, L. N. Hulley, Z. Wu, and W. Shepherd, "Thyristor switch model for power electronic circuit simulation in modified SPICE2," IEEE Trans.Power Electronic, vol.7, no.3, pp.568, 1992.

[A10] J. Bernardes, and D. Dahlgren, "Modeling and analysis of thyristor and diode reverse recovery in railgun pulsed power circuits," in Proc. Conf. on Pulsed Power, pp. 79-82, Montery, USA, 2005.

[A11] Zhou C-N, Yue R-F, Wang Y, Zhang J, Dai G, Li J-T ,"10-kV 4H-SiC gate turn-off thyristors with space-modulated buffer trench three-step JTE". IEEE Electron Device Letters 39:1199–1202, 2018.

[A12] A. K. Agarwal, Q. C. J. Zhang, R. Callanan, C. Capell, A. A. Burk, "9 kV,1cm2 SiC gate turn-off thyristors" in Materials Science Forum, (1017–1020), 2010.

[A13] S.R.Sanders, "Justification of the Describing Function Method for Periodically Switched Circuits", IEEE Conf., pp. 1887-1890, 1992.

[A14] S. Chiniforoosh, J. Jatskevich, V. Dinavahi, R. Iravani, J. A. Martinez, A. Ramirez, "Dynamic average modeling of line-commutated converters for power systems" IEEE General Meeting, PES '09,(1-8), July 2009.